

SUPPORTING INFORMATION

One-step laser nanostructuring of reduced graphene oxide films embedding metal nanoparticles for sensing application

Annalisa Scroccarello^{a,b,‡}, Ruslan Álvarez-Diduk^{a,‡,}, Flavio Della Pelle^b, Cecilia de Carvalho*

Castro e Silva^{a,c}, Andrea Idil^a, Claudio Parolo^a, Dario Compagnone^b, and Arben Merkoçi^{a,d,}*

^aNanobioelectronics & Biosensors Group, Catalan Institute of Nanoscience and Nanotechnology

(ICN2) CSIC and BIST, Campus UAB, 08193 Bellaterra (Barcelona), Spain

^bFaculty of Bioscience and Technology for Food, Agriculture and Environment, University of

Teramo, Campus “Aurelio Saliceti” Via R. Balzarini 1, 64100, Teramo, Italy

^cMackGraphe – Mackenzie Institute for Research in Graphene and Nanotechnologies, Mackenzie

Presbyterian University, Consolação street 930, 01302-907 São Paulo, Brazil

^dICREA Institució Catalana de Recerca i Estudis Avançats, Passeig Lluís Companys 23, 08010

Barcelona, Spain

**Corresponding Authors E-mails: ruslan.alvarez@icn2.cat, arben.merkoci@icn2.cat*

TABLE OF CONTENTS

SM 1.1. Reagents and stock solutions	3
SM 1.2. Samples processing and fogging treatment	3
SM 2. Laser treatment optimization on the graphene oxide film	4
SM 3. Optimization of the MNPs@rGO film fabrication	5
SM 4. Supplementary figures	7
SM 5. Supplementary tables	16

SM 6. Supplementary video

22

References

23

SM 1.1. Reagents and stock solutions

Graphene oxide (GO) suspension (10 mg mL^{-1}) was taken from Angstrom Materials, solution N002-PS-1.0. Ethanol, methanol, silver nitrate (AgNO_3 , > 99%), tetrachloroauric acid trihydrate ($\text{HAuCl}_4 \cdot 3\text{H}_2\text{O}$, 99.9%), potassium tetrachloroplatinate(II) (K_2PtCl_4 , 98%), hexaammineruthenium(III) chloride ($[\text{Ru}(\text{NH}_3)_6]\text{Cl}_3$, 98%), potassium chloride (KCl), sodium phosphate monobasic monohydrate ($\text{NaH}_2\text{PO}_4 \cdot \text{H}_2\text{O}$), sodium phosphate dibasic anhydrous (Na_2HPO_4), caffeic acid, hydrogen peroxide (H_2O_2), sodium nitrite (NaNO_2), sulfuric acid (H_2SO_4 , 99.9%), potassium hexacyanoferrate (III) ($\text{K}_3\text{Fe}(\text{CN})_6$) and potassium hexacyanoferrate (II) trihydrate ($\text{K}_4\text{Fe}(\text{CN})_6 \cdot 3\text{H}_2\text{O}$) were purchased from PanReac AppliChem ITW Reagents (Barcellona, Spain). Carbon sensor paste (C2030519P4), grey dielectric paste (D2070423P5), and silver paste (C2100203D2) were purchased from Gwent group/Sun Chemical (Pontypool, U.K.). The PVDF membrane ($0.1 \mu\text{m}$ of pore size, 47 mm of diameter) and polyethylene terephthalate (PET) sheets were bought from Millipore (Massachusetts, USA) and ADVANCED MICRODEVICES PVT.LTD (Haryana, India), respectively. All the solutions were prepared with Milli-Q water (Purelab OptionQ).

SM 1.2. Samples processing and fogging treatment

The coffee powder has been extracted according to Della Pelle et al. ¹. In brief, 500 mg of coffee powder was weighted and extracted in 10 mL of MeOH:H₂O (80:20) under stirring for 1 hour, in the dark at room temperature. The extract was centrifuged for 10 min (4500 rcf), then the supernatant was collected and filtered with a PTFE syringe filter (VWR, Milan, Italy; Ø = 0.45 µm); the coffee extract was stored at -20°C. Before analysis, the sample was diluted in PB (pH 7.0) to fit the calibration linear range; the caffeic acid quantification was performed by DPV using the standard additions method. The data obtained were expressed as caffeic acid equivalents.

Fishing lake water (Lago Paradiso, Mosciano Sant'Angelo, Teramo, Italy) was collected and filtered with filter paper to remove impurities. Before analysis, the sample was diluted in PB (pH 4.0) to fit the calibration linear range. The nitrite quantification was performed by DPV using the standard additions method.

Fogging in-door disinfection treatment was performed according to Scroccarello et al. ² A solution of H₂O₂ at the recommended concentration (50 g L⁻¹) was freshly prepared and fogged in the analytical chemistry laboratory of the University of Teramo (Teramo, IT, Italy). A commercial 'fogger' (Portable Nano Atomizer, from Migaven) was used to generate an H₂O₂ aerosol of 500 mg m⁻³. The H₂O₂ surface residues were evaluated by placing a surface delimiter realized by adhesive

stencil (sampling area of 2 cm²) onto a laboratory desk before disinfection. After the fogging treatment, 200 µL of PB (pH 7.0) were placed in the surface delimiter, and after 1 min 100 µL were collected and used for the amperometric quantification. The H₂O₂ residues quantification was performed by chronoamperometry (see *section Electrochemical measurements*), and recovery studies were performed directly spiking H₂O₂ onto the surface-delimiter. The analysis was performed in triplicate using three different surface-delimiter, through the standard additions method.

SM 2. Laser treatment optimization on the graphene oxide film

The CO₂ laser power and scan rate were tested in the 2.0-2.5 W and 1.35-1.50 m s⁻¹ range, respectively. Figure S1 reports the GO film before (Figure S1A) and after the laser writing (figure S1B) obtained with the optimal laser power (2.1 W) and scan rate (1.50 m s⁻¹).

The color change from brownish to black/dark grey of the laser-reduced working electrode (key lock geometry) confirms the occurrence of the reduction process.³ Figure S1C reports a magnification of the profile of the laser-treated pattern, where is also evident the high resolution of the CO₂-laser evinced by the boundary between the smooth GO and wrinkled rGO.

For power values lower than 2.1 W no GO reduction occurs, whereas higher values burnt the GO film. While speed rates lower than 1.50 m s⁻¹ induced localized burns on the GO film caused by the high power of the laser.

SM 3. Optimization of the MNPs@rGO film fabrication

The concentration of the metal salt (M^{n+}) to be integrated on the GO during the co-filtration was optimized for the three studied metals. Au(III) and Ag(I) were studied between 3-50 mM, while Pt(II) was between 3-30 mM; for Pt(II) no concentrations higher than 30 mM were explored because the Pt(II) chelate properties strongly induce GO aggregation and sedimentation. Afterward, the film was reduced using the optimized parameters and integrated onto the sensors as described in the main text (*Sensors fabrication*); the result obtained are summarized in Table S1.

Cyclic voltammetry using the parameters reported in Figure 5A-C was run focusing attention on the characteristic peaks of the respective metals. For all the tested metal amounts MNPs formation occurs. The metal salt amount was finally selected according to the best compromise between peak intensity and reproducibility, measuring 5 different electrodes. 30 mM for Au(III) and Pt(II), and 15 mM for Ag(I) were selected as precursor concentrations. In all the cases, lower amounts of metal

precursor produced a scarce and non-reproducible MNPs formation resulting in low current density, whereas higher amounts gave rise to very heterogeneous metallic decorations (Table S1).

To maximize the MNPs decoration and the MNPs@rGO film transferability, different GO amounts at the final concentration of 0.4, 0.8, and 1.6 mg mL⁻¹ were tested. The procedure followed is the one described in the main text *section Laser-assisted MNPs@rGO film formation*, in this case, 30 mM Au(III) was used. Moving the GO concentration from 0.4 mg mL⁻¹ to 1.6 mg mL⁻¹ the number and size of AuNPs increase until their coalescence, up to lead to nanoparticle island/aggregate formation (Table S1). Further, the GO film obtained at 0.4 mg mL⁻¹ resulted too thin to be properly engraved with the CO₂-laser, while for the GO at 1.6 mg mL⁻¹ the presence of the Au islands does not allow uniform transfer onto the sensor substrate.

Finally, the effect of the number of laser reducing cycles was also evaluated. 5 cycles were tested since a higher number of cycles drive to the complete degradation/burst of the film. At increasing reducing cycles a reduction in the AuNPs density was observed (Table S1); the AuNPs deficiencies were attributed to the excess of the photothermal energy provided by the consecutive engraving cycles, that act as an ablation process. For this reason, the laser reducing cycles was fixed to one.

SUPPLEMENTARY FIGURES

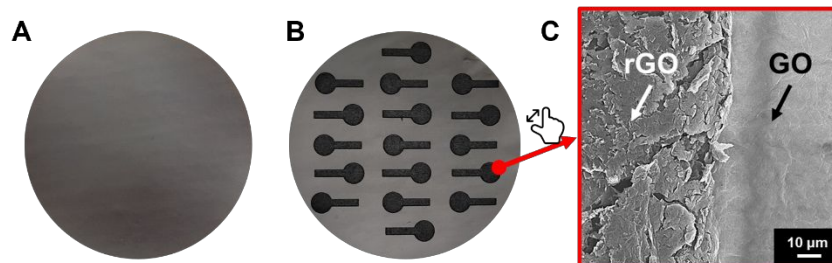


Figure S1. (A) GO-film before and (B) after the laser writing process performed with the optimal laser power (2.1 W) and scan rate (1.50 m s^{-1}). (C) SEM magnification of the profile of laser-reduced pattern.

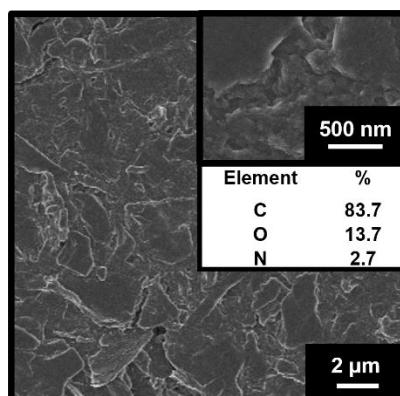


Figure S2. SEM micrograph of the GO-film before the laser scribing process. The inset reports a magnification of the rGO film and the % elemental composition.

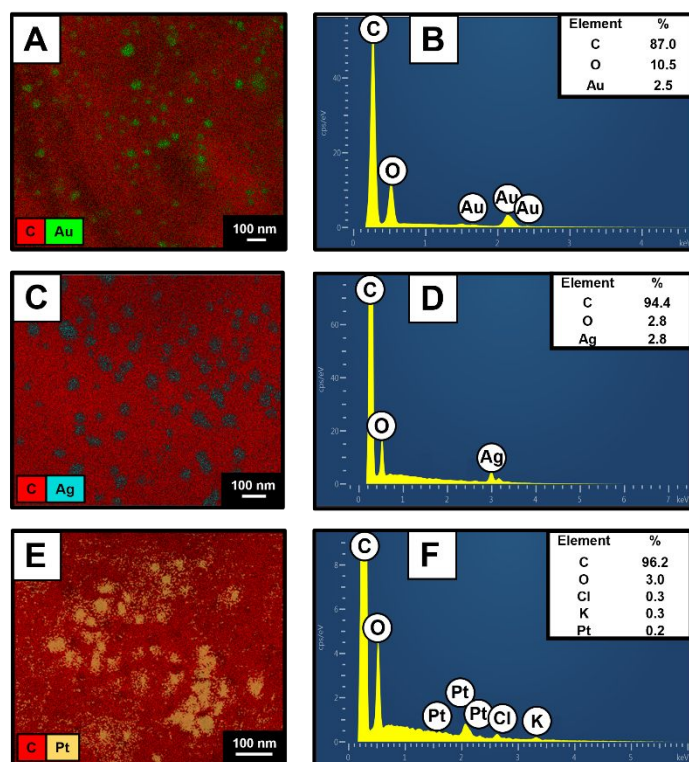


Figure S3. (A) Elemental mapping of (Carbon and Au) of the Au@rGO film and (B) respective EDX analysis. (C) Elemental mapping of (Carbon and Ag) of the Ag@rGO film and (D) respective EDX analysis. (E) Elemental mapping of (Carbon and Pt) of the Pt@rGO film and (F) respective EDX analysis. The micrographs and the EDX analysis were acquired once the MNPs@rGO film was transferred onto the flexible electrode base.

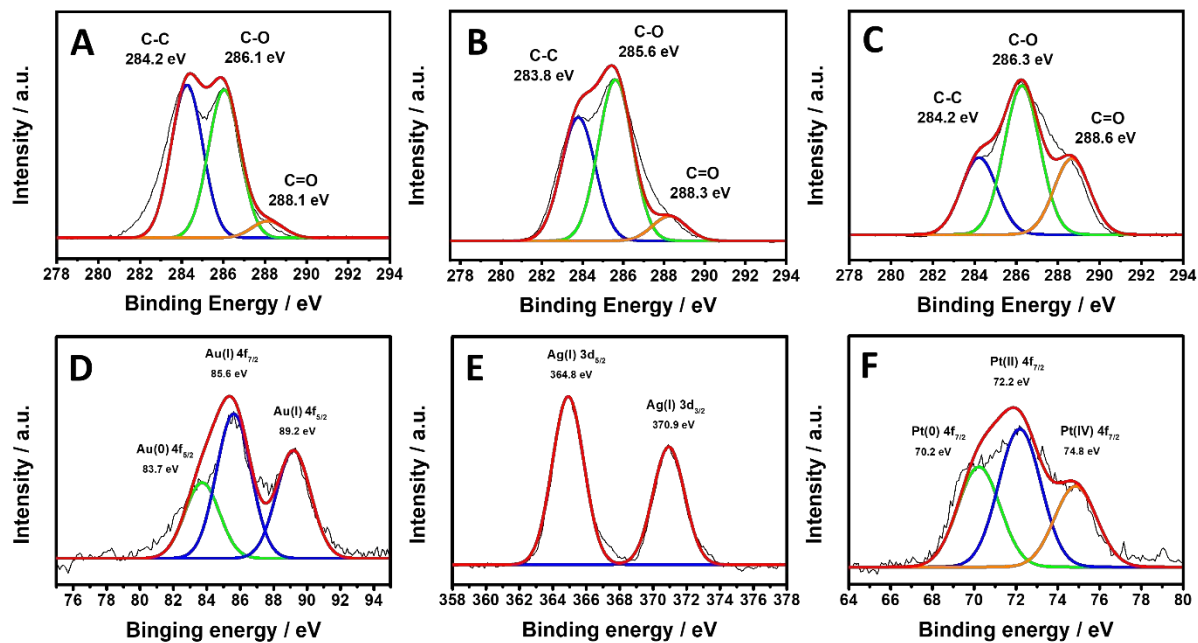


Figure S4. XPS spectra of the $M^{n+}@GO$ films before the laser scribing process. C1s XPS spectrum of the (A) Au(III)@GO, (B) Ag(I)@GO film, (C) and Pt(II)@GO films. Au4f, Ag3d, and Pt4f XPS spectrum of the (D) Au(III)@GO, (E) Ag(I)@GO film, (F) and Pt(II)@GO films, respectively.

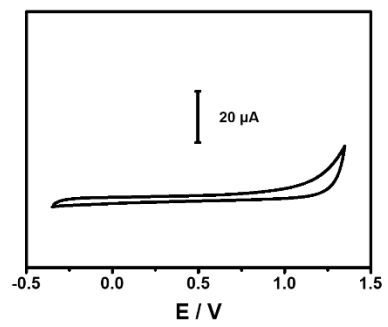


Figure S5. (A) cyclic voltammogram of the rGO sensor in 0.1 M KCl at 100 mV s^{-1} .

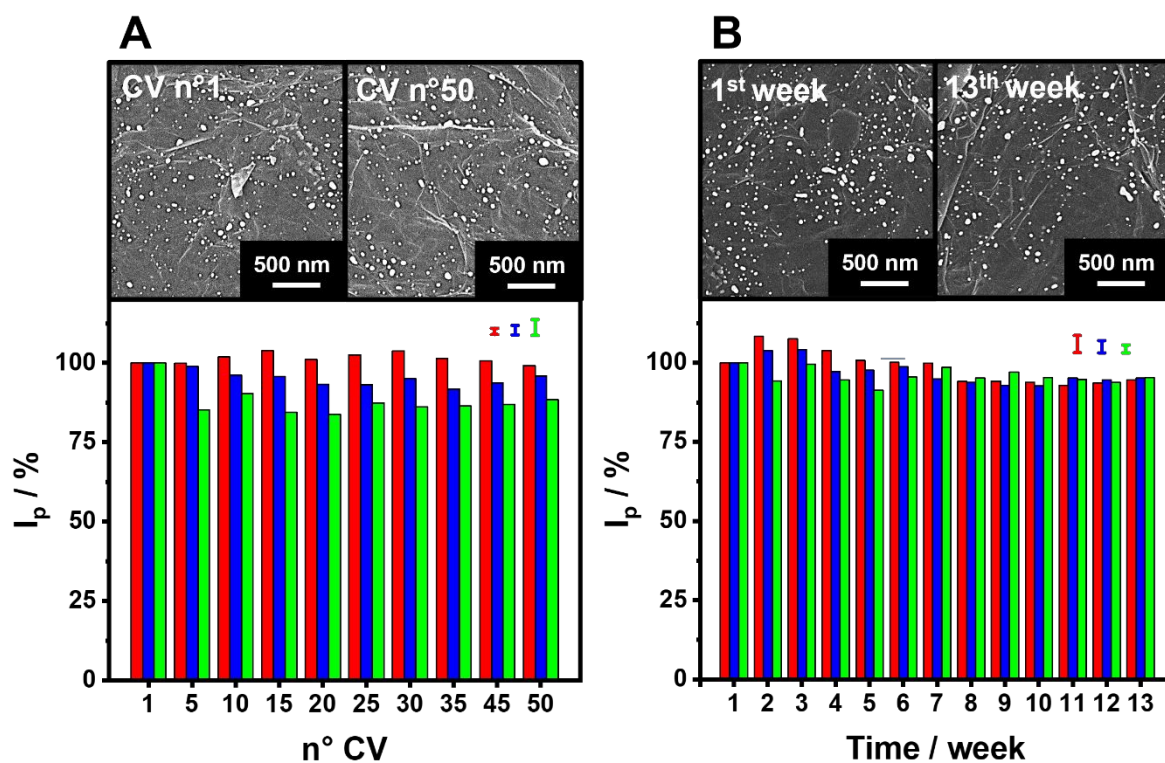


Figure S6. Au@rGO (red bar), Ag@rGO (blu bar), and Pt@rGO (green bar) sensors stability (A) and storability (B). Insets report SEM micrograph of the Au@rGO-film before and after performing 50 CVs (A) and storage (B). Peak intensity expressed as % value and extrapolated from CVs performed with Au@rGO, Ag@rGO, and Pt@rGO sensors in 0.5 M H₂SO₄, 0.1 M KCl, and 0.5 M H₂SO₄, respectively. All the sensors' CVs were performed at 100 mV s⁻¹. In the graph are reported the relative standard deviation bar calculated from the extrapolated peak intensities.

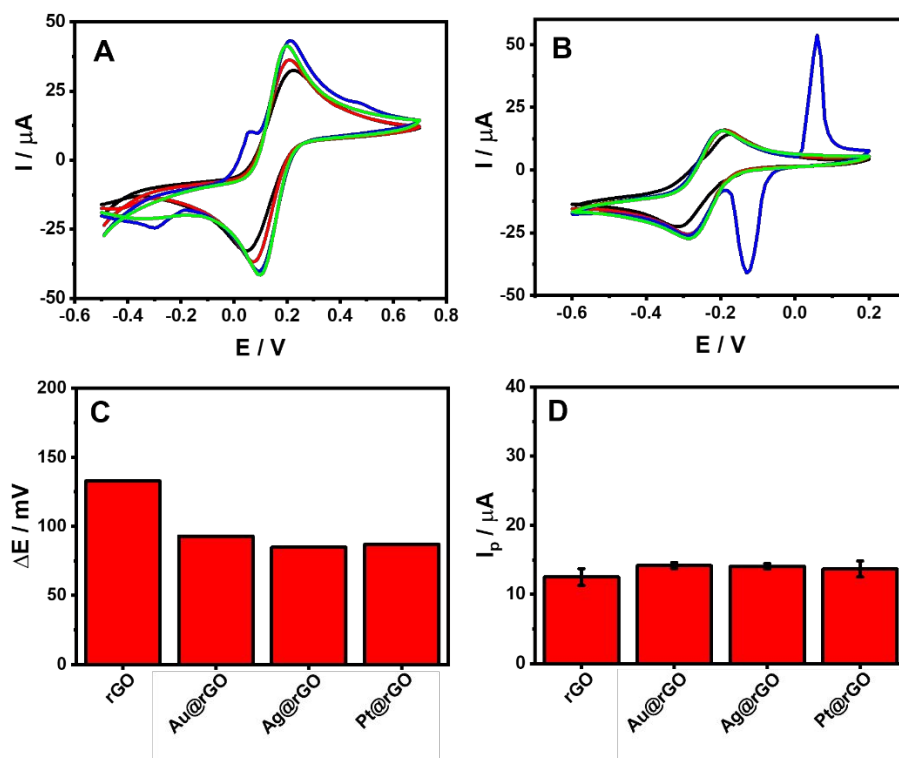


Figure S7. (A) Cyclic voltammograms of (A) 3 mM $\text{Fe}(\text{CN})_6^{4-}/3- in 0.1 \text{ M KCl}$ and (B) 3 mM $\text{Ru}(\text{NH}_3)_6^{3+/2+}$ in 0.1 M KCl performed with the sensors integrating the films of rGO (black line), Au@rGO (red line), Ag@rGO (blue line), and Pt@rGO (green line). (C) Peak-to-peak separation (ΔE) and (D) anodic peak intensity extrapolated from the CVs performed with 3 mM $\text{Ru}(\text{NH}_3)_6^{3+/2+}$ in 0.1 M KCl. The CVs were performed at 25 mV s^{-1} .

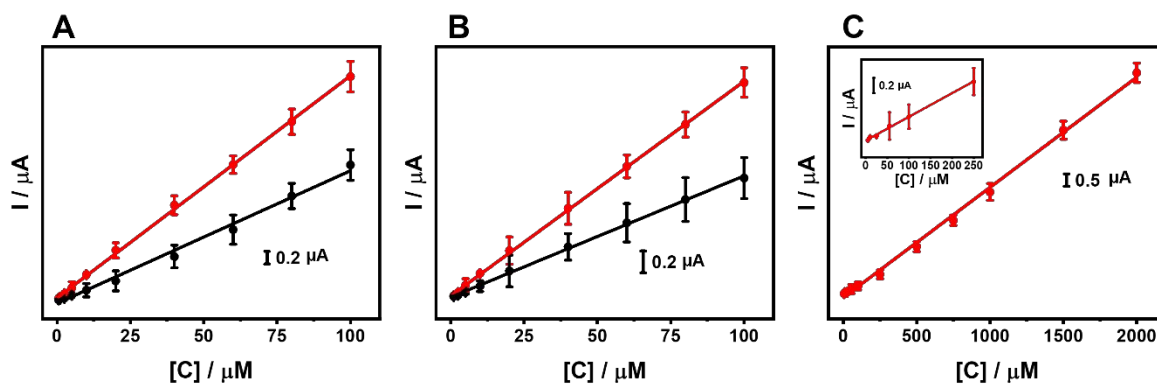


Figure S8. (A) CA calibration curves (0.5-100 μM) performed with the Au@rGO ($y / \mu\text{A} = 0.0351x / \mu\text{M} + 0.0298 / \mu\text{A}$, $R^2 = 0.999$, red line) and rGO ($y / \mu\text{A} = 0.0232x / \mu\text{M} - 0.0672 / \mu\text{A}$, $R^2 = 0.993$, black line) based sensors. (B) NO_2^- calibration curves (1 to 100 μM) performed with the Ag@rGO ($y / \mu\text{A} = 0.0197x / \mu\text{M} + 0.0117 / \mu\text{A}$; $R^2 = 0.999$, red line) and rGO ($y / \mu\text{A} = 0.0111x / \mu\text{M} + 0.0002 / \mu\text{A}$, $R^2 = 0.998$, black line) based sensors. (C) H_2O_2 calibration curve (5-2000 μM) performed with Pt@rGO based sensor ($y / \mu\text{A} = 0.0045x / \mu\text{M} - 0.1274 / \mu\text{A}$, $R^2 = 0.997$, red line).

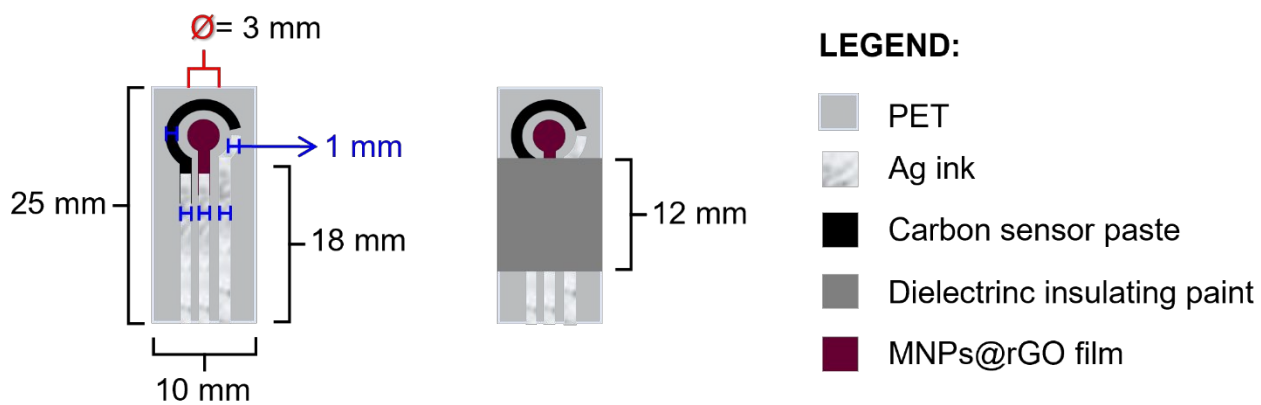
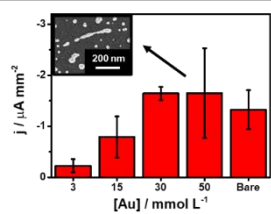
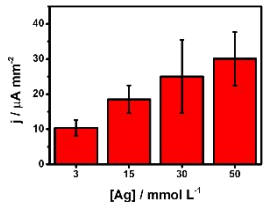
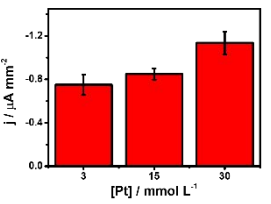
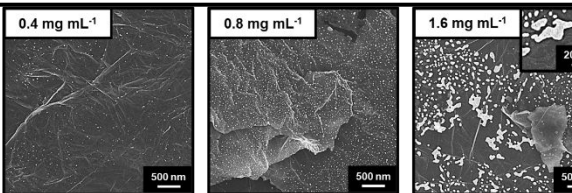


Figure S9. Sensor components' size.

SUPPLEMENTARY TABLES

Table S1. Optimization of the metal precursor amount, graphene oxide amount, and laser reducing cycles

MNPs formation			
[M ⁿ⁺]	Range	Results	Optimal
[Au(III)]	3-50 mM		30 mM
[Ag(I)]	3-50 mM		15 mM
[Pt(II)]	3-30 mM		30 mM
GO concentration			
[GO]	Results		Optimal
0.4, 0.8, 1.6 mg mL ⁻¹			0.8 mg mL ⁻¹

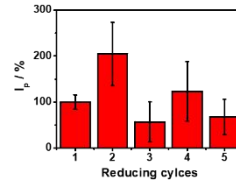
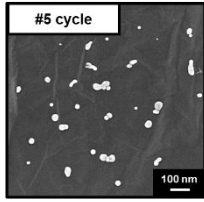
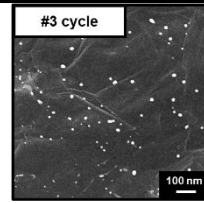
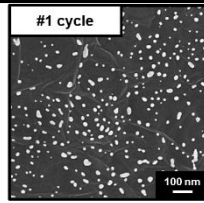
Laser reducing cycle

cycle

Results

Optimal

1-5



1

Table S2. Electrochemical features of the rGO and MNPs@rGO-based sensors.

	OX peak				Ip ratio	ΔE (V)
	Potential	RSD	Intensity	RSD		
	(V)	(%)	(μA)	(%)		
Fe(CN)₆^{2-/3-}						
rGO	0.223 \pm 0.006	2.6	22.3 \pm 3.3	14.7	1.02	0.173
Au@rGO	0.207 \pm 0.009	4.6	26.4 \pm 2.3	8.6	0.99	0.137
Ag@rGO	0.213 \pm 0.006	2.7	29.6 \pm 4.7	16.0	1.00	0.117
Pt@rGO	0.199 \pm 0.008	4.1	29.5 \pm 3.2	10.8	0.92	0.100
Ru(NH₃)₆^{3+/2+}						
rGO	-0.177 \pm 0.012	6.5	12.5 \pm 1.2	9.7	0.97	0.133
Au@rGO	-0.194 \pm 0.011	5.9	14.2 \pm 0.4	3.1	0.90	0.093
Ag@rGO	-0.200 \pm 0.000	0.1	14.1 \pm 0.4	3.0	0.98	0.085
Pt@rGO	-0.198 \pm 0.005	2.5	13.7 \pm 1.2	8.4	0.96	0.087

Table S3. CA-equivalents and NO₂⁻ determination in coffee and fishing lake water sample, respectively. H₂O₂ surface residues determination after fogging treatments.

Sensor	Sample/Application	Added (μM)	Found (μM)	Recovery (%)	RSD (%)	
<i>Au@rGO</i>	Coffee	Caffeic acid				
		-	4.1 ± 0.5	-	12.2	
		7.5	7.8 ± 0.6	103	7.7	
		10	10.3 ± 1.1	102	10.7	
		12.5	13.8 ± 1.2	110	8.7	
<i>Ag@rGO</i>	F. lake water	NO ₂ ⁻				
		-	<LOD	-		
		5	5.2 ± 0.4	104	7.7	
		10	11.9 ± 1.1	109	9.2	
		20	20.3 ± 2.1	101	10.3	
<i>Pt@rGO</i>	Fogging treatment	H ₂ O ₂				
		Time 0	-	65.5 ± 4.5	-	6.9
			20	19.6 ± 1.3	98	6.6
			40	36.9 ± 3.1	92	8.4
			60	58.5 ± 6.1	98	10.4

Time 15 min	-	21.1 ± 2.4	-	11.4
	20	20.9 ± 1.7	104	8.1
	40	38.7 ± 4.1	97	10.6
	60	65.8 ± 6.9	110	10.5
Time 30 min	-	14.6 ± 1.8	-	12.3
	20	21.6 ± 3.2	108	14.8
	40	35.9 ± 3.8	90	10.6
	60	67.0 ± 5.1	112	7.6

Table S4. Electrochemical performance comparison of rGO or laser-induced graphene-based electrodes.

Electrode	Decoration strategy	Analyte	Detection method	Linear range (μM)	LOD (μM)	Ref.
PEDOT*– LIG**	-	DA***	DPV	1-150	0.33	4
LIG	-	DA	DPV	0.5-32	0.27	5
Pt@LIG	Electrodep.	DA	DPV	0.5-56	0.07	
Au@rGO	Laser scribing	CA	DPV	0.5-100	0.05	This work
LIG	-	NO_2^-	DPV	2-1000	0.90	6
			LSV	200-4000	1.18	
ZnO@rGO	Ultra-sonication	NO_2^-	Amperom. (1.1 V)	20-520	1.36	7
Ag@rGO	Laser scribing	NO_2^-	DPV	1-100	0.12	This work
Cu–Ru@LIG	Laser scribing	H_2O_2	Amperom. (-0.4 V)	10-4320	1.8	8
Ag@rGO	Electrodep.	H_2O_2	Amperom. (-0.5 V)	100-10000	7.5	9
Pt@LIG	Sputtering	H_2O_2	Amperom. (-0.2 V)	0.5–5000	0.20	10

Pt@rGO	Laser scribing	H ₂ O ₂	Amperom. (0.0 V)	5-2000	0.64	This work
--------	----------------	-------------------------------	---------------------	--------	------	-----------

* PEDOT: poly(3,4-ethylenedioxythiophene)

**LIG: Laser-induced graphene

*** DA: dopamine

Video 1. rGO-based conductive film patterning, fabrication, and transferring onto flexible PET substrate

References

- (1) Della Pelle, F.; Scroccarello, A.; Sergi, M.; Mascini, M.; Del Carlo, M.; Compagnone, D. Simple and Rapid Silver Nanoparticles Based Antioxidant Capacity Assays: Reactivity Study for Phenolic Compounds. *Food Chem.* **2018**. <https://doi.org/10.1016/j.foodchem.2018.02.141>.
- (2) Scroccarello, A.; Della Pelle, F.; Del Carlo, M.; Compagnone, D. Monitoring Disinfection in the Covid-19 Era. A Reagent-Free Nanostructured Smartphone-Based Device for the Detection of Oxidative Disinfectants. *Microchem. J.* **2022**, *175* (November 2021), 107165. <https://doi.org/10.1016/j.microc.2021.107165>.
- (3) Giacomelli, C.; Alvarez-Diduk, R.; Testolin, A.; Merkoci, A. Selective Stamping of Laser Scribed RGO Nanofilms: From Sensing to Multiple Applications. *2D Mater.* **2020**, *7* (2), 024006. <https://doi.org/10.1080/00480169.2014.948521>.
- (4) Xu, G.; Jarjes, Z. A.; Desprez, V.; Kilmartin, P. A.; Travas-Sejdic, J. Sensitive, Selective, Disposable Electrochemical Dopamine Sensor Based on PEDOT-Modified Laser Scribed Graphene. *Biosens. Bioelectron.* **2018**, *107* (November 2017), 184–191. <https://doi.org/10.1016/j.bios.2018.02.031>.
- (5) Nayak, P.; Kurra, N.; Xia, C.; Alshareef, H. N. Highly Efficient Laser Scribed Graphene Electrodes for On-Chip Electrochemical Sensing Applications. *Adv. Electron. Mater.* **2016**, *2* (10). <https://doi.org/10.1002/aelm.201600185>.
- (6) Zhang, N.; Yang, J.; Hu, C. Laser-Scribed Graphene Sensors on Nail Polish with Tunable Composition for Electrochemical Detection of Nitrite and Glucose. *Sensors Actuators B Chem.* **2022**, *357* (January), 131394. <https://doi.org/10.1016/j.snb.2022.131394>.
- (7) Rashed, M. A.; Faisal, M.; Harraz, F. A.; Jalalah, M.; Alsaiani, M.; Al-Assiri, M. S. RGO/ZnO/Nafion Nanocomposite as Highly Sensitive and Selective Amperometric Sensor for Detecting Nitrite Ions (NO₂⁻). *J. Taiwan Inst. Chem. Eng.* **2020**, *112*, 345–356. <https://doi.org/10.1016/j.jtice.2020.05.015>.
- (8) Thirumalai, D.; Lee, J. U.; Choi, H.; Kim, M.; Lee, J.; Kim, S.; Shin, B. S.; Chang, S. C. In Situsynthesis of Copper-Ruthenium Bimetallic Nanoparticles on Laser-Induced Graphene

- as a Peroxidase Mimic. *Chem. Commun.* **2021**, *57* (15), 1947–1950. <https://doi.org/10.1039/d0cc07518c>.
- (9) Aparicio-Martínez, E.; Ibarra, A.; Estrada-Moreno, I. A.; Osuna, V.; Dominguez, R. B. Flexible Electrochemical Sensor Based on Laser Scribed Graphene/Ag Nanoparticles for Non-Enzymatic Hydrogen Peroxide Detection. *Sensors Actuators, B Chem.* **2019**, *301* (May), 127101. <https://doi.org/10.1016/j.snb.2019.127101>.
- (10) Zhang, Y.; Zhu, H.; Sun, P.; Sun, C. K.; Huang, H.; Guan, S.; Liu, H.; Zhang, H.; Zhang, C.; Qin, K. R. Laser-Induced Graphene-Based Non-Enzymatic Sensor for Detection of Hydrogen Peroxide. *Electroanalysis* **2019**, *31* (7), 1334–1341. <https://doi.org/10.1002/elan.201900043>.